The Astrophysical Journal Letters, 743:L24 (4pp), 2011 December 10 doi:10.1088/2041-8205/743/1/L24

RAPID FLUCTUATIONS IN THE LOWER SOLAR ATMOSPHERE

J. K. Lawrence[1], A. C. Cadavid[1], D. J. Christian[1], D. B. Jess[2], and M. Mathioudakis[2]
[1] Department of Physics and Astronomy, California State University, Northridge, Northridge, CA 91330-8268, USA; john.lawrence@csun.edu
[2] Astrophysics Research Centre, School of Mathematics and Physics, Queen's University Belfast, Belfast, BT7 1NN, UK
Received 2011 October 1; accepted 2011 November 7; published 2011 November 22

ABSTRACT

The Rapid Oscillations in the Solar Atmosphere instrument reveals solar atmospheric fluctuations at high frequencies. Spectra of variations of the *G*-band intensity (I_G) and Ca II K-line intensity (I_K) show correlated fluctuations above white noise to frequencies beyond 300 mHz and 50 mHz, respectively. The noise-corrected *G*-band spectrum for $f = 28$–326 mHz shows a power law with exponent -1.21 ± 0.02, consistent with the presence of turbulent motions. *G*-band spectral power in the 25–100 mHz ("UHF") range is concentrated at the locations of magnetic bright points in the intergranular lanes and is highly intermittent in time. The intermittence of the UHF *G*-band fluctuations, shown by a positive kurtosis κ, also suggests turbulence. Combining values of I_G, I_K, UHF power, and κ reveals two distinct states of the solar atmosphere. State 1, including almost all the data, is characterized by low I_G, I_K, and UHF power and $\kappa \approx 6$. State 2, including only a very small fraction of the data, is characterized by high I_G, I_K, and UHF power and $\kappa \approx 3$. Superposed epoch analysis shows that the UHF power peaks simultaneously with spatio-temporal I_G maxima in either state. For State 1, I_K shows 3.5 minute chromospheric oscillations with maxima occurring 21 s after I_G maxima implying a 150–210 km effective height difference. However, for State 2 the I_K and I_G maxima are simultaneous; in this highly magnetized environment sites of *G*-band and K-line emission may be spatially close together.

Key words: Sun: chromosphere – Sun: oscillations – Sun: photosphere

Online-only material: animation

1. INTRODUCTION

As solar observations with increasing spatial and temporal resolution become available, the search continues for an energy supply to balance radiative losses in the chromosphere. Of renewed interest are contributions from high-frequency magnetoacoustic fluctuations. Bello Gonzalez et al. (2010) using Doppler images from the IMaX two-dimensional spectropolarimeter on board *Sunrise*, with spatial resolution 100–130 km, found an energy flux of ~7000 W m^{-2} in the 5.2–10 mHz range. This is half of the highest radiative loss estimate of 14,000 W m^{-2} (Anderson & Athay 1989). High-frequency ($f > 10$ mHz) magnetoacoustic waves also may play an important role in chromospheric heating. Hasan et al. (2005) and Hasan & van Ballegooijen (2008) analyzed photospheric motions and found it reasonable to expect turbulent velocity fluctuations in intergranular lanes with timescales ~20 s and that these fluctuations might buffet the footpoints of magnetic flux tubes producing upward propagating hydromagnetic waves. They therefore proposed that chromospheric heating could occur due to waves with frequencies greater than 10 mHz.

Frequencies as high as 100 mHz have been detected in *Transition Region and Coronal Explorer* data (DeForest 2004), but the detection of high-frequency waves has been difficult because of atmospheric seeing and space-based instrumental and telemetry limitations (e.g., Fossum & Carlsson 2006). Now, however, the required observations with higher spatial and time resolution are more readily available (Carlsson et al. 2007) with the advent of faster CCDs and improved image reconstruction.

Here, we use data obtained with the Rapid Oscillations in the Solar Atmosphere (ROSA) instrument (Jess et al. 2010) at the Dunn Solar Telescope (DST) to identify high-frequency fluctuations in both the photosphere and upper photosphere/chromosphere. We investigate the temporal and spatial properties of the fluctuations and test them against the properties predicted in the model of Hasan and van Ballegooijen (2008). We do not anticipate wave-like oscillations at high frequencies, but rather intermittent and turbulent fluctuations in the photosphere, manifested by power-law spectra.

2. OBSERVATIONS

Images were obtained with the ROSA instrument on 2009 May 28 (Jess et al. 2010). A sequence of exceptionally good seeing and alignment covered 32 Mm square at disk center and spanned 32.34 minutes. We use observations taken in the *G* band of the CH radical at 4305.5 Å, bandpass 9.2 Å, with exposure times 15 ms at a cadence of 30.3 frames s^{-1}. These were reconstructed to a cadence of 0.525 s. We also use images in the Ca II K-line core at 3933.7 Å, bandpass 1.0 Å, with cadence 4.2 s. High-order adaptive optics (AO) corrected wave front deformations in real time (Rimmele 2004), and the images underwent photometrically accurate speckle reconstruction (Weigelt & Wirnitzer 1983; Wöger et al. 2008) to reach spatial resolution 100 km (Figure 1). In the present work, the *G*-band images were averaged to a 1.05 s cadence for calculating the spectrum and a 4.2 s cadence otherwise.

3. ANALYSIS AND RESULTS

3.1 Identification of Ultra High Frequencies

We calculated the complex Morlet wavelet transform $W(t, \tau)$ of the intensity time signals at every spatial location and each time step. The spectral power is $P = |W(t, \tau)|^2$, and τ is the period (Torrence & Compo 1998). We averaged over spacetime voxels excluding those within 3.5 minutes from the ends of the

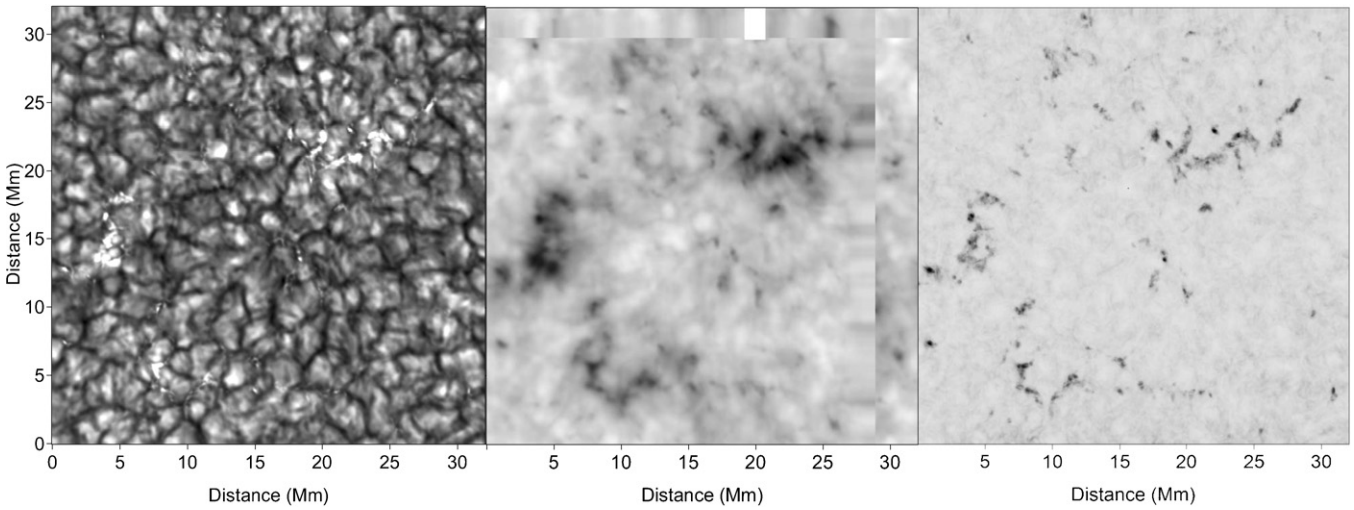

Figure 1. Time average of (left) the *G*-band intensity images, (middle) the Ca II K-line intensity with the gray scale inverted, and (right) the spectral power of 25–100 mHz *G*-band fluctuations, also with gray scale reversed. The K-line image has been shifted to align with the *G*-band image.

(An animation of this figure is available in the online journal.)

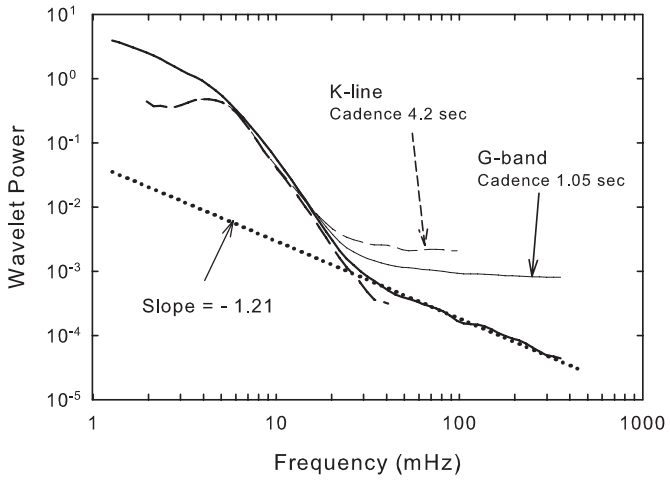

Figure 2. Morlet wavelet spectra averaged over spacetime points throughout the data block. Thin solid line: raw *G*-band spectrum at cadence 1.05 s. Thin dashed line: raw K-line spectrum at cadence 4.2 s. The thick solid and dashed lines are the noise filtered spectra of *G* band and K-line, respectively. The dotted line represents a best fit to the *G*-band power law for $f = 28$–326 mHz.

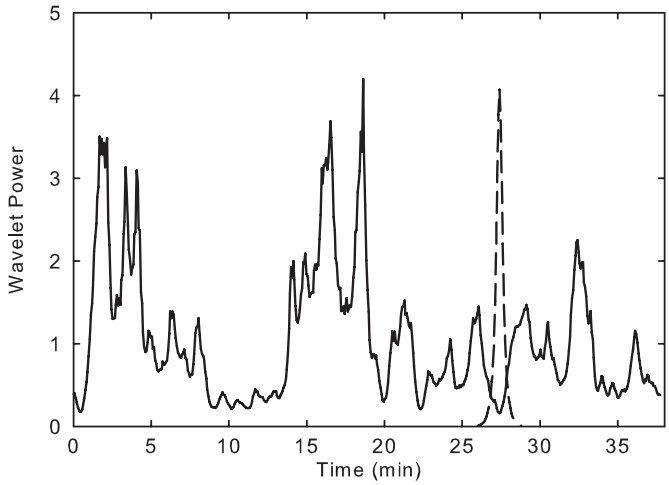

Figure 3. Time dependence of the UHF *G*-band spectral power at one spatial location corresponding to a *G*-band bright point and at 4.2 s cadence (solid line). The dashed line is the spectral response to a delta-function intensity impulse.

data string. This gives the raw spectra in Figure 2 shown as a thin solid line for *G* band and a thin dashed line for K-line. The K-line and *G*-band fluctuations at cadences of 4.2 s and 1.05 s, have Nyquist frequencies of 120 mHz and 480 mHz, respectively. Uncorrelated (white) noise produces a flat spectrum. The raw *G*-band spectrum in Figure 2 flattens above 300 mHz, and the K-line above 50 mHz. Since the white noise must be uncorrelated with any signal, the noise contribution to the spectrum can be subtracted off (Press et al. 1989). We model the *G*-band spectral power for high frequencies as a power law in frequency with exponent $-\alpha$ plus a constant chosen to minimize the uncertainty of α. Then a fit over the range $28 < f < 326$ mHz (more than a decade in frequency) gives $\alpha = 1.21 \pm 0.02$. The corrected *G*-band spectrum is shown in Figure 2 as a thick solid line. The power-law fit is shown by a dotted line. The similarly corrected *K*-line spectrum has a maximum corresponding to 3.5 minute oscillations, then falls off with a power-law spectrum with index $\alpha \approx 4$. This is shown as a heavy dashed line.

To study their physical origin, we integrated the *G*-band spectra at each spacetime voxel over the 25–100 mHz band, which we arbitrarily call the "UHF" band, and averaged over time. The UHF power is widely distributed in area, but strong concentrations (Figure 1) appear at the locations of *G*-band bright points in the intergranular lanes. We associate the bright points with magnetic flux tubes and refer to them as "magnetic bright points" (MBPs). The UHF concentrations also align closely with the bright cores of the K-line emission (Figure 1).

Wavelets can analyze signals in both frequency and time. Figure 3 shows a time plot of the UHF *G*-band wavelet power at the spatial location of an MBP. The highly intermittent variations are clear. See the animation in the online journal.

3.2. UHF and Intensity

We studied various quantities as functions of the *G*-band intensity (I_G). I_G was divided into bins of width 0.01 in arbitrary units. Then, sampling all spacetime voxels in the corresponding data cube gives the mean of the K-line intensity (I_K) in each bin. After multiplication by an arbitrary factor for convenience

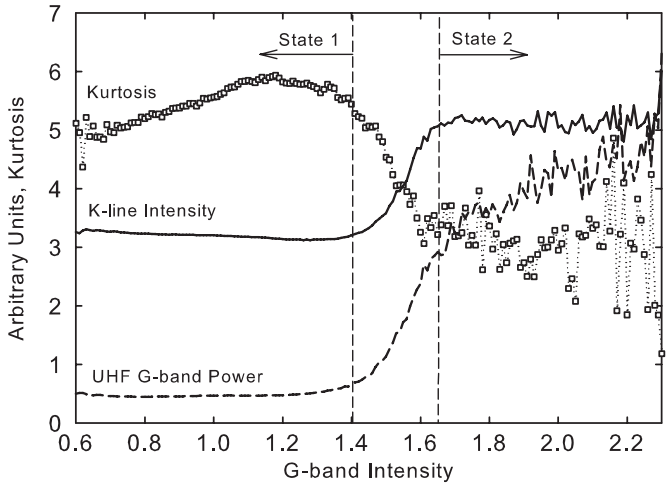

Figure 4. K-line intensity (solid), *G*-band UHF spectral power (dashed), and kurtosis of the *G*-band fluctuations filtered to the UHF frequencies (open squares) vs. *G*-band intensity in bins of 0.01. The *G*-band and K-line intensities and the UHF power are in arbitrary units. The kurtosis is a dimensionless number. The sizes of local error bars are well indicated by the short-term scatter in the plots.

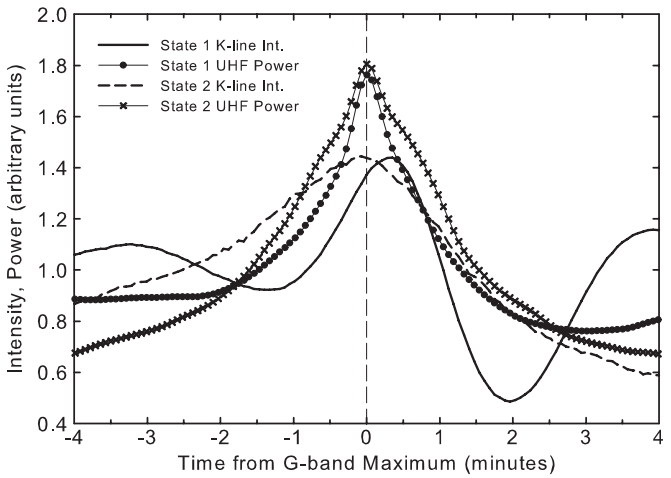

Figure 5. Averaged plots of I_K and *G*-band UHF power zeroed on times of maximum I_G. The solid curve and the filled circles correspond to the requirement that the maxima belong to State 1 and represent I_K and *G*-band UHF power, respectively. The dashed line and $\times$'s represent the same for State 2. The units of all the variables are arbitrary and have been adjusted for clarity of display.

of display, the solid curve in Figure 4 shows the mean I_K as a function of I_G. There is a lower plateau for $0.6 \leqslant I_G \leqslant 1.4$, a transition, and then a higher plateau for $I_G \geqslant 1.65$. For convenience, we call these cases "State 1" and "State 2," respectively. Although the transition of the mean I_K appears continuous, a plot of the full histograms indicates that in the transition the population of points with lower I_K decreases as I_G increases above 1.4, while a population of points with greater I_K appears and increases in number. This suggests two distinct states of the solar atmosphere. State 1 includes 98.6% of all data voxels, State 2 only 0.15%.

We next investigated the dependence on I_G of the UHF *G*-band power. The wavelet spectra are normalized by the square of the mean I_G at the spatial location where the spectrum is calculated. This is to offset bias in the UHF spectra caused by the magnitude of the intensity. The dashed line in Figure 4 shows a plateau in State *I*, then a steep linear transition, followed by a reduced-slope linear dependence in State 2. This again points to two distinct states. In contrast, the 3–5 mHz power spectrum (not shown) does not have a well-defined transition, although it does increase for larger I_G.

Still more can be learned about the processes underlying the fluctuations by studying the shapes of their distribution functions. The kurtosis κ of a distribution is its fourth moment about the mean divided by the second moment squared, all minus 3. With this definition the κ of a Gaussian distribution is zero. Distributions with $\kappa < 0$ have truncated tails, such as for harmonic oscillations. Distributions with $\kappa > 0$ have heavy tails. These indicate intermittency and are found, for example, in turbulent motions. In Figure 4, we have plotted the kurtosis of the I_G fluctuations, after filtering to the UHF bandpass, and averaging in each I_G bin. For State 1, κ lies between values of 5 and 6. Then there is a clear transition, and in State 2 κ drops to a value around 3. We thus find that the UHF fluctuations are intermittent in both States 1 and 2. In State 1 the fluctuations are highly intermittent and suggest the presence of turbulent motions. In State 2 the fluctuations are still intermittent, although less so. These may reflect the buffeting of magnetic flux elements by turbulence. In the case of *G*-band 3–5 mHz fluctuations (not shown) we find that $\kappa \approx -1$ over the whole range of I_G. This indicates a truncated distribution and implies harmonic oscillations.

3.3. Superposed Epoch Analysis

The relative timing of fluctuations in I_G and I_K were best studied by superposed epoch analysis (Lühr et al. 1998). This simple method is used when there are many observations of a certain kind of event and one wants to investigate the real responses minus any noise. By averaging over many cases the real signal remains while the noisy contributions are suppressed. In the present example, we first locate local spatio-temporal maxima of I_G. In each such case we record the I_G time series for four minutes before and after the maximum, which is taken as the zero point. We record the simultaneous values of the I_K time series, and the *G*-band UHF power series, each with the same zero point. We repeat this for all I_G maxima meeting some criterion, such as that the maximum lies in State 1, and then average the I_G, I_K and the UHF spectral power series within each time bin 4.2 s apart. Overall, we find 446,431 qualifying maxima in State 1 and 5585 in State 2.

Figure 5 shows the resulting plots made separately for States 1 and 2. The two plots for UHF power each have a peak at $t = 0$, coincident with the local I_G maxima. The UHF spectra have been normalized with respect to the mean I_G at each spatial location. In State 1 the I_K plot shows oscillations with period about 3.5 minutes, consistent with the chromospheric oscillations. The maximum of I_K is delayed after the I_G maximum by 21 s. For State 2, no I_K oscillations are apparent in our eight-minute window, and the I_K maximum is simultaneous with the I_G maximum.

4. SUMMARY AND DISCUSSION

We identified significant power for fluctuations in I_K beyond 50 mHz, and in I_G beyond 300 mHz. Jess et al. (2007) identified frequencies up to 50 mHz in *G*-band and Hα observations made with the Rapid Dual Imager, a predecessor of ROSA.

After correction for white noise, we obtained power-law spectra. For 28 mHz $< f <$ 326 mHz the *G*-band spectrum has index $\alpha = 1.21 \pm 0.02$. This indicates scale invariance and because α is different from 0 (white noise) and 2 (Brownian

motion) it points to a nonlinear process such as chaos or turbulence (Bak et al. 1987). Using I_G as a proxy for the strength of the magnetic field (Schüssler et al. 2003), we found that the UHF *G*-band fluctuations were spatially associated with MBPs in the intergranular lanes as well as with K-line bright cores. Lawrence et al. (2001) had earlier found that the spatial and temporal scaling of MBP motions resembled the walks of imperfectly correlated tracers of turbulent fluid flow in intergranular lanes.

With corrected ground-based observations come concerns about residual seeing effects. In this case, the atmospheric seeing was optimal, and the application of high-order AO correction, photometrically accurate speckle reconstruction, and a dense 40×40 de-stretching grid, should remove all residual feature displacements. The KISIP speckle reconstruction code (Wöger et al. 2008) has been checked for photometric accuracy against contemporaneous space-based *Hinode*/SOT-FG images.

We have checked the possibility that the association of UHF power with the small MBPs might be a feature-size-dependent scintillation effect. The increase of high-frequency *G*-band spectral power of our State 2 over that of State 1 (Figure 4) actually begins at 10 mHz and is fully present by 30 mHz. We can just reach this range in a few *Hinode* data sets, and we find there the same association of spectral power with MBPs as here. This result would not be affected by terrestrial seeing.

We encountered two distinct states of the solar atmosphere (Figure 4). State 1 defined by $I_G = 0.6$–1.4 contained 98.6% of the data. It showed relatively low mean I_K and UHF spectral power. State 2 defined by $I_G \geqslant 1.65$ contained only 0.15% of the data and showed strongly increased mean I_K and mean UHF spectral power. Previous work (Schrijver et al. 1989; Rezaei et al. 2007; Loukitcheva et al. 2009) found that network features showed a power-law relation between the photospheric magnetic field strength and the intensity of Ca II K-line emission. In contrast, we find a definite transition between the two "states" that occurs in the range $1.4 \leqslant I_G \leqslant 1.65$. This same transition is found in *Hinode*/SOT-FG images of internetwork. The Ca II H-line intensity undergoes a step increase as *G*-band intensity increases past a critical value. In the case of network, however, after the step increase, the H-line intensity resumes increasing as *G*-band intensity increases.

For data filtered to the 3–5 mHz frequency band the kurtosis κ indicates a harmonic signal. For the UHF frequency band κ corresponds to an intermittent time series as illustrated in Figure 4. This provides further evidence that the UHF signal is neither uncorrelated noise nor harmonic oscillations but rather the result of a chaotic or turbulent process. The amplitude of the UHF fluctuations in State 1 is small compared to State 2, but the signal is still present and has a greater kurtosis.

Superposed epoch analysis showed that for both States 1 and 2 the UHF power of the I_G fluctuations peaked simultaneously with I_G itself. For State 1 I_K shows a 3.5 minute oscillation and has a maximum 21 s after the I_G maximum. In the case of State 2, the I_K shows no oscillation and its peak appears simultaneous with that of I_G.

In State 1 the I_G and I_K fluctuations give information on both the turbulent driving motions and the propagating acoustic wave. A time delay of 21 s and a velocity of 7–10 km s^{-1} imply a height separation of 150–210 km between the *G*-band and K-line sources. Using data obtained with the Interferometric Bidimensional Spectrometer at DST and assuming the 1-D FALC model of a static solar atmosphere (Fontenla et al. 1991), Reardon et al. (2009) found that the Ca II K-line response function peaks near a height of 400 km. Rimmele (2004), using the Universal Birefringent Filter at DST, found that the *G* band forms in the mid-photosphere near 200 km. Thus, our K-line observations appear dominated by an upper photospheric signal. For State 2 no delay appears between the *G*-band and K-line maxima. In this active, highly magnetized environment, the geometrical configuration of the atmosphere may be sufficiently disturbed that sites of G-band and K-line emission lie spatially close together. This is an open question, of course, and requires further investigation.

Taken together, the following results: scale invariance, nonlinearity, and intermittence of the UHF *G*-band fluctuations evoke the model described by Hasan et al. (2005) and Hasan & van Ballegooijen (2008) in which magneto-acoustic waves with frequencies above 10 mHz are generated by the interaction of flux tubes with turbulent downflows in the intergranular lanes.

Observations were obtained at the National Solar Observatory, operated by the Association of Universities for Research, in Astronomy, Inc. (AURA), under agreement with the National Science Foundation. D.J.C. thanks California State University, Northridge for startup funds.

REFERENCES

Anderson, L. S., & Athay, R. G. 1989, ApJ, 346, 1010
Bak, P., Tang, C., & Wiesenfeld, K. 1987, Phys. Rev. Lett., 59, 381
Bello Gonzalez, N., Franz, M., Martínez Pillet, V., et al. 2010, ApJ, 723, L134
Carlsson, M., Hansteen, V. H., de Pontieu, B., et al. 2007, PASJ, 59, S663
DeForest, C. E. 2004, ApJ, 617, L89
Fontenla, J. M., Avrett, E. H., & Loeser, R. 1991, ApJ, 377, 712
Fossum, A., & Carlsson, M. 2006, ApJ, 646, 579
Hasan, S. S., & van Ballegooijen, A. A. 2008, ApJ, 680, 1542
Hasan, S. S., van Ballegooijen, A. A., Kalkofen, W., & Steiner, O. 2005, ApJ, 631, 1270
Jess, D. B., Andic, A., Mathioudakis, M., Bloomfield, D. S., & Keenan, F. P. 2007, A&A, 473, 943
Jess, D. B., Mathioudakis, M., Christian, D. J., et al. 2010, Solar Phys., 261, 363
Lawrence, J. K., Cadavid, A. C., Ruzmaikin, A. A., & Berger, T. E. 2001, Phys. Rev. Lett., 86, 5894
Loukitcheva, M., Solanki, S. K., & White, S. M. 2009, A&A, 497, 273
Lühr, H., Rother, M., Iyemori, T., Hansen, T. L., & Lepping, R. P. 1998, Ann. Geophys., 16, 743
Press, W. H., Flannery, B. P, Teukolsky, S. A., & Vetterling, W. T. 1989, Numerical Recipes in C (Cambridge: Cambridge Univ. Press)
Reardon, K. P., Uitenbroek, H., & Cauzzi, G. 2009, A&A, 500, 1239
Rezaei, R., Schlichenmaier, R., Beck, C. A. R., Bruls, J. H. M. J., & Schmidt, W. 2007, A&A, 466, 1131
Rimmele, T. 2004, ApJ, 604, 906
Schrijver, C. J., Cote, J., Zwaan, C., & Saar, S. H. 1989, ApJ, 337, 964
Schüssler, M., Shelyag, S., Berdyugina, S., Vögler, A., & Solanki, S. K. 2003, ApJ, 597, L173
Torrence, C., & Compo, G. P. 1998, Bull. Am. Meteor. Soc., 79, 61
Weigelt, G., & Wirnitzer, B. 1983, Opt. Lett., 8, 389
Wöger, F., von der Lühe, O., & Reardon, K. 2008, A&A, 488, 375